Am J Physiol Endocrinol Metab 316: E475–E486, 2019.
First published January 8, 2019; doi:10.1152/ajpendo.00380.2018.

RESEARCH ARTICLE

Calcium signaling and secretory granule pool dynamics underlie biphasic insulin secretion and its amplification by glucose: experiments and modeling

Morten Gram Pedersen,[1,2,3] Alessia Tagliavini,[1] and Jean-Claude Henquin[4]

[1]*Department of Information Engineering, University of Padova, Padova, Italy;* [2]*Department of Mathematics "Tullio Levi-Civita," University of Padova, Padova, Italy;* [3]*Padova Neuroscience Center, University of Padova, Padova, Italy; and* [4]*Unit of Endocrinology and Metabolism, Faculty of Medicine, University of Louvain, Brussels, Belgium*

Submitted 6 September 2018; accepted in final form 7 January 2019

Pedersen MG, Tagliavini A, Henquin JC. Calcium signaling and secretory granule pool dynamics underlie biphasic insulin secretion and its amplification by glucose: experiments and modeling. *Am J Physiol Endocrinol Metab* 316: E475–E486, 2019. First published January 8, 2019; doi:10.1152/ajpendo.00380.2018.—Glucose-stimulated insulin secretion from pancreatic β-cells is controlled by a triggering pathway that culminates in calcium influx and regulated exocytosis of secretory granules, and by a less understood amplifying pathway that augments calcium-induced exocytosis. In response to an abrupt increase in glucose concentration, insulin secretion exhibits a first peak followed by a lower sustained second phase. This biphasic secretion pattern is disturbed in diabetes. It has been attributed to depletion and subsequent refilling of a readily releasable pool of granules or to the phasic cytosolic calcium dynamics induced by glucose. Here, we apply mathematical modeling to experimental data from mouse islets to investigate how calcium and granule pool dynamics interact to control dynamic insulin secretion. Experimental calcium traces are used as inputs in three increasingly complex models of pool dynamics, which are fitted to insulin secretory patterns obtained using a set of protocols of glucose and tolbutamide stimulation. New calcium and secretion data for so-called staircase protocols, in which the glucose concentration is progressively increased, are presented. These data can be reproduced without assuming any heterogeneity in the model, in contrast to previous modeling, because of nontrivial calcium dynamics. We find that amplification by glucose can be explained by increased mobilization and priming of granules. Overall, our results indicate that calcium dynamics contribute substantially to shaping insulin secretion kinetics, which implies that better insight into the events creating phasic calcium changes in human β-cells is needed to understand the cellular mechanisms that disturb biphasic insulin secretion in diabetes.

β-cells; calcium dynamics; exocytosis; mathematical model; pancreatic islets

INTRODUCTION

Glucose-induced insulin secretion requires operation of two complementary mechanisms in pancreatic β-cells: an increase in the cytosolic free calcium concentration $[Ca^{2+}]_i$ that triggers exocytosis of insulin granules and actuation of an amplifying pathway that augments the exocytotic response to calcium (25). The amplifying signals derive from glucose metabolism, but their exact biochemical nature is still uncertain (15, 25, 33).

It has long been known that a rapid and sustained increase in blood glucose induces a biphasic rise in plasma insulin concentrations in normal human subjects (5, 7). This peculiar insulin kinetics is due to the biphasic dynamics of insulin secretion by pancreatic β-cells, as calculated by C-peptide deconvolution (62, 63) and directly established by in vitro studies using isolated human islets (26, 56). Although produced only by unphysiologically rapid glucose stimulations, this biphasic insulin response of β-cells has attracted considerable attention because a low first phase has proved to be predictive of a deterioration of glucose homeostasis (8, 45, 54). In patients with impaired glucose tolerance or overt diabetes, both phases are impaired (19, 30, 52, 54) with sometimes (62, 64), though not always (19, 30), a greater impact on the first phase. Elucidation of the cellular mechanisms underlying biphasic insulin secretion thus has clinical implications. Achieving such a goal, however, rests on accessible experimental models.

A biphasic dynamics also characterizes glucose-induced plasma insulin changes (29, 46) and in vitro insulin secretion (11, 35, 37) in rodents. To explain the two phases of insulin secretion observed in the perfused rat pancreas, Grodsky (21, 22) proposed a model in which a limited pool of readily releasable insulin "packets" was secreted quickly to create the first phase, and subsequent refilling of the pool was responsible for the second phase. He also modeled the so-called staircase protocol in which the glucose stimulus is increased in small steps, each giving rise to a first phase-like peak of insulin, by assuming that the readily releasable insulin pool is heterogeneous, containing insulin packets with different glucose-thresholds (21). According to an alternative model proposed by Cerasi et al. (6), the two phases of insulin secretion result from the interaction of inhibitory and potentiating signals with different kinetics. Subsequent studies (36, 47) compared the storage- and signal-limited models, found that both have caveats, and concluded that a combined model with both limited insulin pools and time-dependent signals performed better. However, the cellular origin of the heterogeneity of the releasable pool of insulin and the biochemical nature of the putative inhibitory and potentiating signals remained elusive.

Studies of exocytosis in single β-cells provided substantial support to the pool model, with depletion of a readily releasable pool (RRP) yielding the first phase and refilling of the RRP creating the second phase (2, 10, 48, 58). It was further suggested that cell-to-cell heterogeneity seen in $[Ca^{2+}]_i$ imaging experiments (32) could underlie the postulated

Address for reprint requests and other correspondence: M. G. Pedersen, Dept. of Information Engineering, Univ. of Padova, Via Gradenigo 6/B, 35131 Padova, Italy (e-mail: pedersen@dei.unipd.it).

threshold distribution for the RRP (50). Although β-cell coupling through gap junctions within islets substantially reduces intercellular heterogeneity (59, 60) and synchronizes cellular responses (49, 55), recent evidence indicates that some heterogeneity persists between β-cells and islets (3, 39), possibly accounting for RRP heterogeneity.

The most obvious signal capable of inducing biphasic insulin secretion is the triggering $[Ca^{2+}]_i$, the increase of which follows a biphasic kinetics in glucose-stimulated β-cells (13, 25, 28). Such a view is supported by experiments showing that all maneuvers interfering with the rapid rise in $[Ca^{2+}]_i$ alter the first phase and that all agents inducing a rapid $[Ca^{2+}]_i$ rise induce a rapid secretion (25, 28). However, observations of biphasic insulin secretion in face of virtually sustained elevations of $[Ca^{2+}]_i$ produced by tolbutamide or KCl speak against this interpretation (28, 43). Whether amplifying signals and/or depletion of a limited amount of releasable insulin contribute to the phasic insulin pattern under these conditions is unclear.

In the present study, we combined experimental measurements of $[Ca^{2+}]_i$ and insulin secretion in mouse islets with mathematical modeling to unravel the contributions of $[Ca^{2+}]_i$ signals and pool dynamics to biphasic insulin secretion. Our analysis shows that triggering signals and granular pools both contribute to shaping the biphasic release pattern and uncover mechanisms underlying amplification by glucose of the secretory response to calcium.

MATERIALS AND METHODS

Experiments

All experiments were performed with islets isolated from the pancreas of female C57BL6 mice. After hand selection, the islets were cultured overnight in RPMI medium containing 10 mM glucose and then used for dynamic measurements of insulin secretion or $[Ca^{2+}]_i$. All methods were exactly as described in our previous studies (29, 43). Because all presented traces correspond to averages of results obtained with several islets, oscillations in $[Ca^{2+}]_i$ and insulin secretion present in individual islets are masked, whereas the biphasic dynamics of these responses are preserved. The study was approved by and experiments were conducted in accordance with the guidelines of the University of Louvain Animal Research Committee.

Mathematical Modeling

Our aim was to study the impact of $[Ca^{2+}]_i$ dynamics on insulin secretion. We developed various models of granule pool dynamics that were driven by the experimentally recorded $[Ca^{2+}]_i$ traces (Fig. 1). Simulated secretion profiles were then fitted to experimental insulin patterns to investigate which models were able to fit the data satisfactorily. The models were described by ordinary differential equations, in which some of the transition rates between different pools depended on the glucose concentration, whereas the combined exocytosis/secretion rate depended on the time-varying, experimentally recorded $[Ca^{2+}]_i$ traces. Parameter estimation was not our scope, and identifiability issues and estimation accuracy were neglected.

Model 1. In this model, only an RRP is present. This pool is refilled from an infinite reserve pool by a "mobilization" or "refilling" process with rate $M(G)$, depending on the glucose concentration G. The RRP granules can undergo fusion and secretion with rate $S(Ca)$, depending linearly on $[Ca^{2+}]_i$ above a threshold (31, 49). Granules can also undergo glucose-independent "internalization" or "loss-of-release capability" with rate N from the RRP. The instantaneous secretion is thus $RRP(t)\cdot S(Ca[t])$. We assume that insulin I to be fitted to the experimental data is measured from a reservoir described by first-order kinetics with a time constant of 1 min, i.e.,

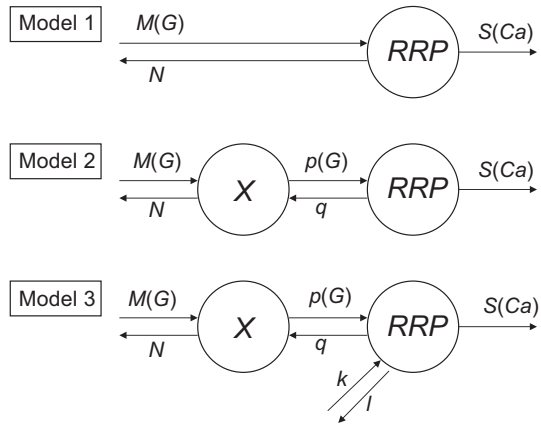

Fig. 1. Overview of the three considered models. RRP, readily releasable pool. $M(G)$, rate of glucose-dependent "mobilization" or "refilling" process; $S(Ca)$, $[Ca^{2+}]_i$-dependent rate of RRP granules fusion and secretion; N, "internalization" or "loss-of-release capability" rate; X, intermediate granule pool; $p(G)$, glucose-dependent priming rate; q, glucose-independent "unpriming" rate; k, rate of glucose-independent mobilization directly to the RRP; l, rate of glucose-independent internalization from the RRP.

$$dI/dt = \left(S \cdot RRP - I\right)/\left(1\ \text{min}\right).$$

This model has 10 parameters to be estimated.

Model 2. This model adds an intermediate pool X located near or at the plasma membrane of Model 1. The granule pool X is refilled from an infinite reserve pool with rate $M(G)$, depending on the glucose concentration G. From the pool X, the granules enter the RRP following glucose-dependent priming with rate $p(G)$. As in Model 1, the RRP granules may be released with rate $S(Ca)$. Granules can also undergo glucose-independent "unpriming" with rate q from the RRP and glucose-independent internalization with rate N from X. Model 2 has 18 parameters to be estimated.

Model 3. In this model, glucose-independent mobilization directly to, and internalization from, the RRP with rate k, respectively l, was added to Model 2. Such direct mobilization bypassing the pool X may represent "basal" mobilization and is accessible to tolbutamide- or potassium-induced $[Ca^{2+}]_i$ elevations. Model 3 has 20 parameters to be estimated.

Data Fitting

For each model, we fixed the parameters and simulated 14 different protocols corresponding to the experimental data. The parameters M and p were allowed to change with glucose levels (assuming the same value for 10 mM and 11.1 mM glucose to reduce the number of parameters to fit). For experiments with prestimulation in 3 mM glucose (rows 1, 3, and 4 in Fig. 2), the initial conditions for the pool sizes were set so that the model was in steady state in the absence of secretion. For experiments with prestimulation in 8.5 mM glucose (row 2 in Fig. 2), the initial conditions were set to the final value of the model simulation after a step from 3 mM to 8.5 mM glucose.

The parameters were then varied automatically within the optimization algorithm, and the simulated secretion data were compared with the experimental recordings to minimize the squared error, calculated as the difference between simulated (I) and experimental insulin data for the 14 protocols. To exploit the information from the relatively few tolbutamide protocols, we weighted the residuals from fitting of the experiments from Mourad et al. (43) 10 times higher.

The procedure was repeated with different initial choices of the parameter set, to reduce the risk of ending in a local minimum, and eventually led to a single parameter vector for which the model fit to the 14 experimental data sets was optimal. Model parameters were constrained so that mobilization and priming were nondecreasing

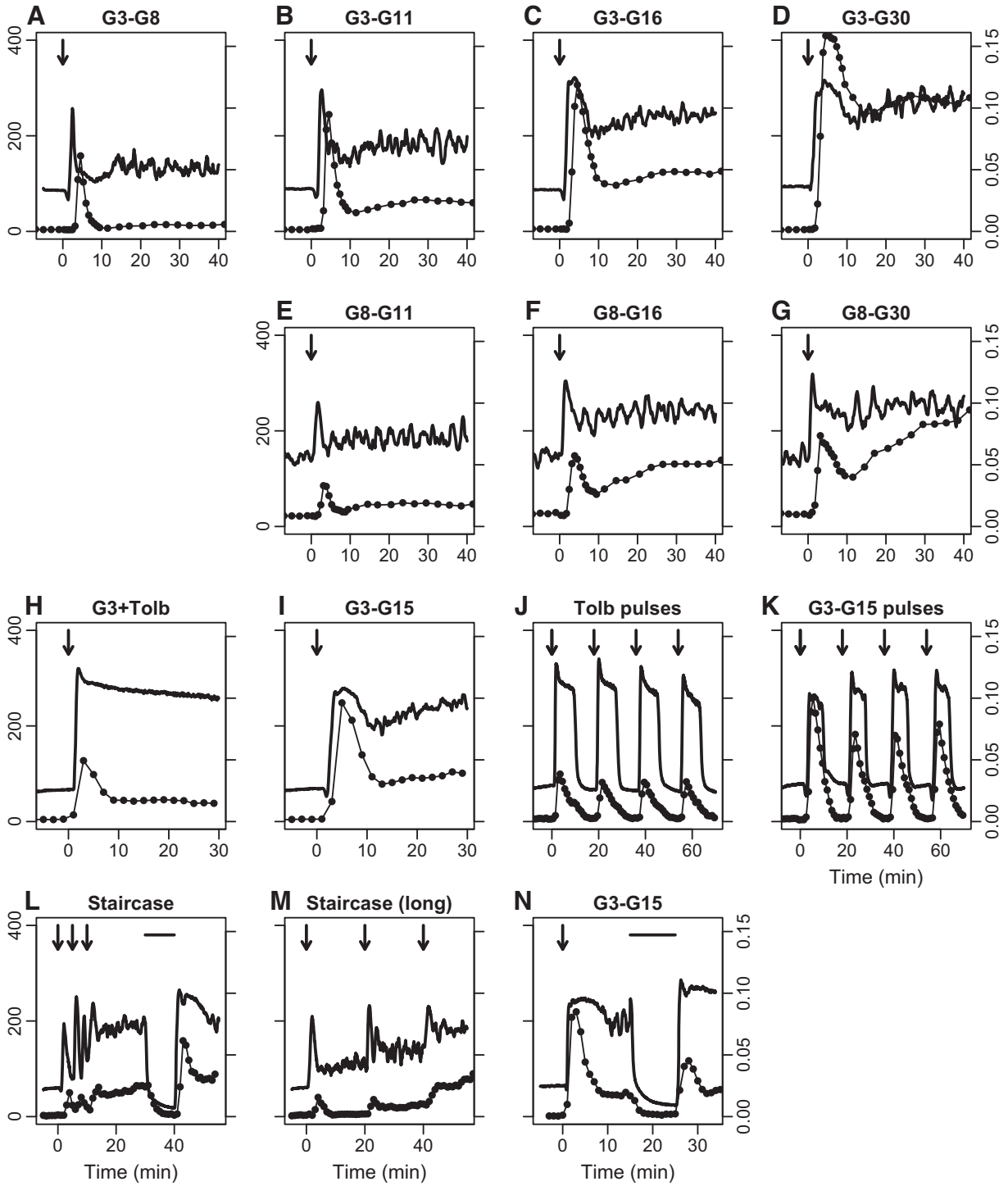

Fig. 2. Experimental data. Experimental $[Ca^{2+}]_i$ traces (in nM; bold curves, left axes) and insulin secretion measurements (% of islet content per minute; thin curves with dots, right axes). Time is in minutes. *A–G*: data are from Henquin et al. (29), in which glucose was stepped at 0 min (indicated by arrow) from 3 mM (*A–D*) or 8.5 mM (*E–G*) to 8.5, 11.1, 16.7, or 30 mM, as indicated. *H–K*: data are from Mourad et al. (43), in which islets were stimulated by either 500 μM tolbutamide (Tolb) in 3 mM glucose or 15 mM glucose continuously or in 8-min pulses, as indicated by arrows. *L–N*: data are new experiments shown as means for 3 experiments of insulin secretion and 12–18 islets for $[Ca^{2+}]_i$. *L*: staircase increased in glucose from 3 mM to 7 mM, 10 mM, and finally 15 mM in 5-min steps, indicated by arrows, followed by removal of extracellular calcium between 30 and 40 min (indicated by the bar). *M*: steps of the staircase were extended to a duration of 20 min, as indicated by arrows. *N*: glucose was stepped from 3 mM to 15 mM at 0 min (arrow), followed by removal of extracellular calcium between 15 and 25 min (bar).

functions of glucose. In other fits, no constraints were imposed, allowing mobilization and priming rates to be nonmonotone functions of glucose, hence permitting extra degrees of freedom for the estimation of parameters.

Simulations were done in MATLAB (version R2017b; Mathworks Inc.) using the ode45 solver. Fitting was performed with the "fmincon" function. The computer code is available at http://www.dei.unipd.it/~pedersen.

RESULTS

Experimental Data Description

We fitted our mathematical models to reproduce results from previously published (29, 43) and novel studies of phasic islet $[Ca^{2+}]_i$ changes and insulin secretion in response to different protocols of glucose or tolbutamide stimulation (Fig. 2).

In a first series of experiments taken from (29), brisk jumps of glucose from 3 mM to 8.5, 11.1, 16.7, or 30 mM in perifusion medium resulted in biphasic insulin secretion and $[Ca^{2+}]_i$ elevation (Fig. 2, *A–D*). The first phases of secretion and $[Ca^{2+}]_i$ increased in both amplitude and duration, with increasing glucose concentration. Second phases of secretion and $[Ca^{2+}]_i$ also increased with glucose. In a second series, islets were initially exposed to 8.5 mM glucose before being stimulated with 11.1, 16.7, or 30 mM glucose (Fig. 2, *E–G*). Both insulin and $[Ca^{2+}]_i$ responses were again biphasic, but first phases were smaller than after initial perifusion in 3 mM glucose, whereas second phases were similar.

A third series of experiments, taken from Ref. 43, compared insulin and $[Ca^{2+}]_i$ responses in islets subjected to stimulation with 15 mM glucose or 500 μM tolbutamide in 3 mM glucose (Fig. 2, *H–K*). Salient differences and similarities were identified. Sustained stimulation with either stimulus induced a clearly biphasic secretion of insulin, although the dynamics of the $[Ca^{2+}]_i$ response evoked by tolbutamide were hardly biphasic compared with that evoked by glucose (Fig. 2, *H* versus *I*). Tolbutamide-induced secretion was ~50% smaller than glucose-induced secretion in the face of a slightly greater elevation of $[Ca^{2+}]_i$, a difference that reflects amplification of insulin secretion by glucose. Application of short pulses of tolbutamide or glucose, to mimic several first phases, again induced roughly similar $[Ca^{2+}]_i$ responses but smaller insulin responses with tolbutamide than glucose (Fig. 2, *J* versus *K*). With each stimulus, the amplitude of the first insulin pulse was slightly larger than that of subsequent pulses.

Finally, in a series of novel experiments, islets were stimulated using staircase increases in glucose concentration from 3 to 7, 10, and eventually 15 mM (Fig. 2, *L–N*). When steps at 7 and 10 mM glucose were short (5 min), a distinct $[Ca^{2+}]_i$ peak was produced by every increase in glucose concentration, which was accompanied by a peak of insulin secretion (Fig. 2*L*). Applying longer glucose steps (20 min) did not substantially change the pattern (Fig. 2*M*); a small second phase evolved at 7 and 10 mM glucose, but the peaks evoked by each increase in glucose had a similar size to the ones evoked by short steps. Notably, the first phase of the $[Ca^{2+}]_i$ response to 15 mM glucose was much longer, though not greater in amplitude, following the single step directly from 3 mM glucose than during the staircase protocol (step from 10 mM glucose), and the corresponding first phase of insulin secretion was considerably larger (Fig. 2*N*). Second phases were similar. Omission of extracellular calcium, while keeping glucose at 15 mM, markedly lowered islet $[Ca^{2+}]_i$ and stopped insulin secretion. Reintroduction of calcium elicited rapid increases in $[Ca^{2+}]_i$ and secretion, but the insulin peak was smaller than that observed after a step from 3 to 15 mM glucose, although the $[Ca^{2+}]_i$ response was not smaller (Fig. 2*N*).

We next used these 14 experimentally recorded $[Ca^{2+}]_i$ traces as inputs to models of insulin release. The simulated secretion profiles were then fitted to the corresponding experimental insulin patterns. As explained above, three models of increasing complexity were compared.

Performance of Model 1

The simple Model 1, with a single pool, fit the data acceptably but underestimated the peaks when glucose was stepped from 3 mM to 8.5, 11.1, 16.7, or 30 mM (Fig. 3, *A–D*, red curves) and overestimated the peak after reintroduction of calcium in 15 mM glucose (Fig. 3, *L* and *N*). This latter discrepancy could be corrected (not shown), in this and in Models 2 and 3 to be discussed below, by assuming a lower refilling rate at low $[Ca^{2+}]_i$ levels (23). During stimulation with 8.5 mM glucose, the RRP was nearly constant (Fig. 4*A*). The smaller size of the peaks observed when stepping to 16.7 or 30 mM glucose occurred from 8.5 mM (Fig. 3, *F* and *G*) rather than 3 mM glucose (Fig. 3, *C* and *D*) was almost entirely due to the shorter duration of the first-phase $[Ca^{2+}]_i$ signals following pre-exposure to 8.5 mM glucose (Fig. 2).

As shown in Fig. 2, *H–K*, tolbutamide in 3 mM glucose evoked slightly larger increases in $[Ca^{2+}]_i$ than 15 mM glucose did, but the resulting secretion of insulin was larger with glucose than tolbutamide; that difference was observed during the two phases of a sustained stimulation and during application of repetitive pulses. Model 1 reproduced these differences reasonably, though the first peak of tolbutamide-stimulated secretion was slightly overestimated (Fig. 3, *H* and *J*), and the first phase of secretion triggered by 15 mM glucose was slightly underestimated (Fig. 3, *I* and *K*) in the model.

Model 1 was also able to reproduce the staircase experiments (Fig. 3, *L* and *M*). In response to each step in glucose, simulated insulin secretion showed a peak, which was driven by $[Ca^{2+}]_i$ dynamics, not pool depletion, since the RRP was nearly constant during the staircase protocols (Fig. 4*F*). This contrasts with Grodsky's model (21), which postulated heterogeneity of the RRP, the peak of secretion induced by each glucose step being attributed to the release of subpools of granules with increasing glucose thresholds. In our model, these insulin peaks were purely due to the peaks in the $[Ca^{2+}]_i$ signal (Fig. 2, *L* and *M*).

The estimated refilling rate remained at the basal value up to ~10 mM glucose, after which it increased, yielding an overall sigmoidal dependence on glucose concentration (Fig. 3*O*, red curve). When the constraint that refilling as a function of glucose be nondecreasing throughout was removed, no noticeable improvement in the model fits was observed, and the overall results were as described above (Fig. 3, blue curves).

Thus, within the physiological range of glucose concentrations, Model 1 predicted that differences in secretion measured in the various protocols were largely due to the different $[Ca^{2+}]_i$ signals. Pool depletion played a role at

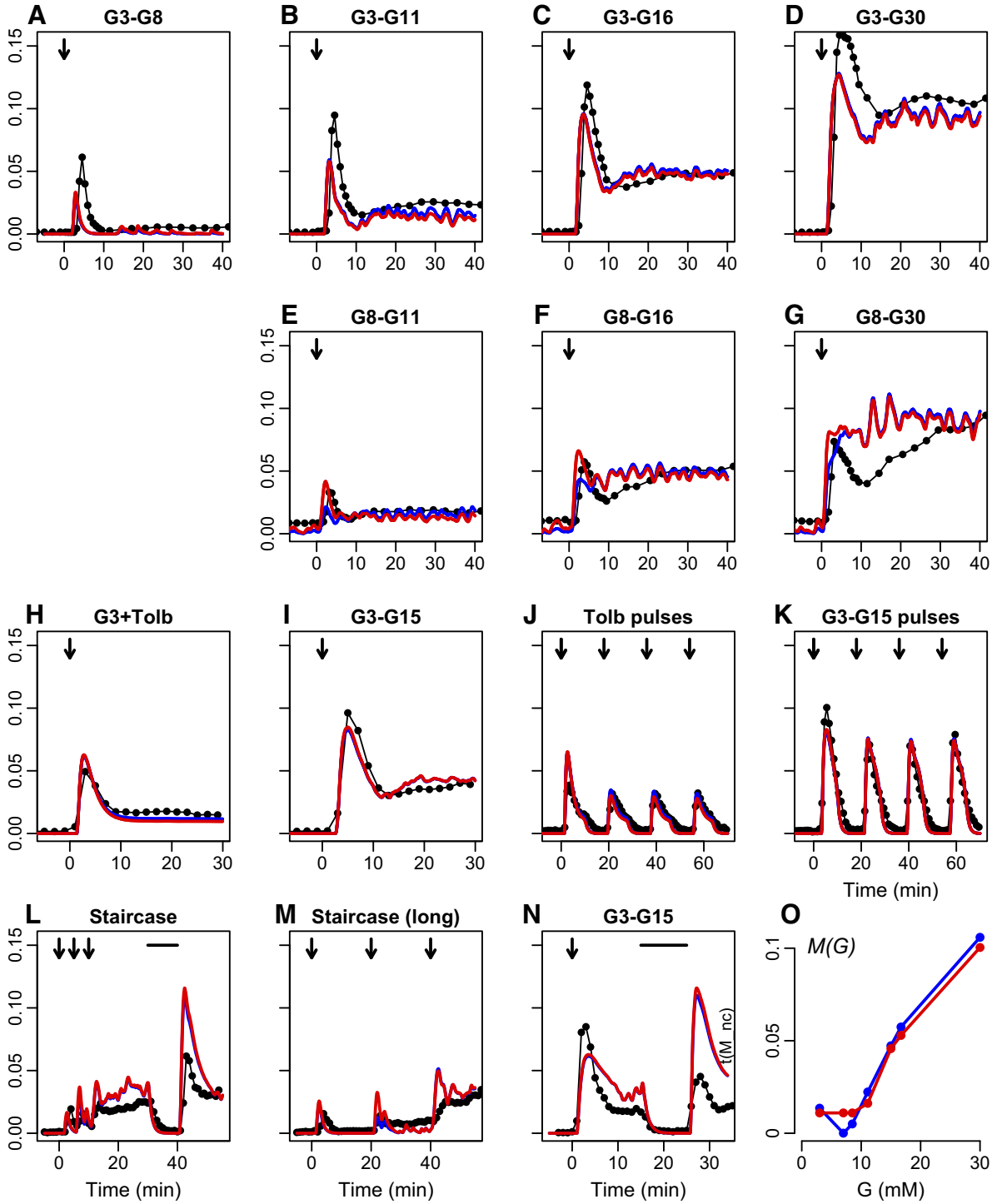

Fig. 3. Model 1 results. Simulated secretion profiles (% of islet content/min; axes are shown only once for each row) obtained with Model 1, fitted to the experimental data (black dots and curves), either with (red curves) or without (blue curves) the constraint of refilling being a nondecreasing function of the glucose concentration *G*. *A*–*N*: layout is the same as in Fig. 2. *O*: parameters for refilling [*M*(*G*) in % of islet content/min] with (red) or without (blue) the monotony constraint on *M*(*G*). *M*(*G*), rate of glucose-dependent refilling process; Tolb, tolbutamide.

higher glucose levels and during tolbutamide stimulation (Fig. 4, *B*, *D*, and *E*).

In the model, tolbutamide acted (via Ca^{2+}) only on secretion *S*(*Ca*), and the relatively low peak of secretion in response to tolbutamide (Fig. 2, *H* and *J*) imposed a limit on the estimate of the initial size of RRP. A limited pool, in turn, resulted in a low simulated peak when glucose was stepped to 8.5 mM (Fig. 3*A*), since the refilling rate *M* could not be too large for the model to reproduce the nearly absent second phase of secretion at 8.5 mM. The same problem was seen at the other levels of glucose. In other words, in this simple Model 1, there was a contradiction between the low peak of secretion seen in re-

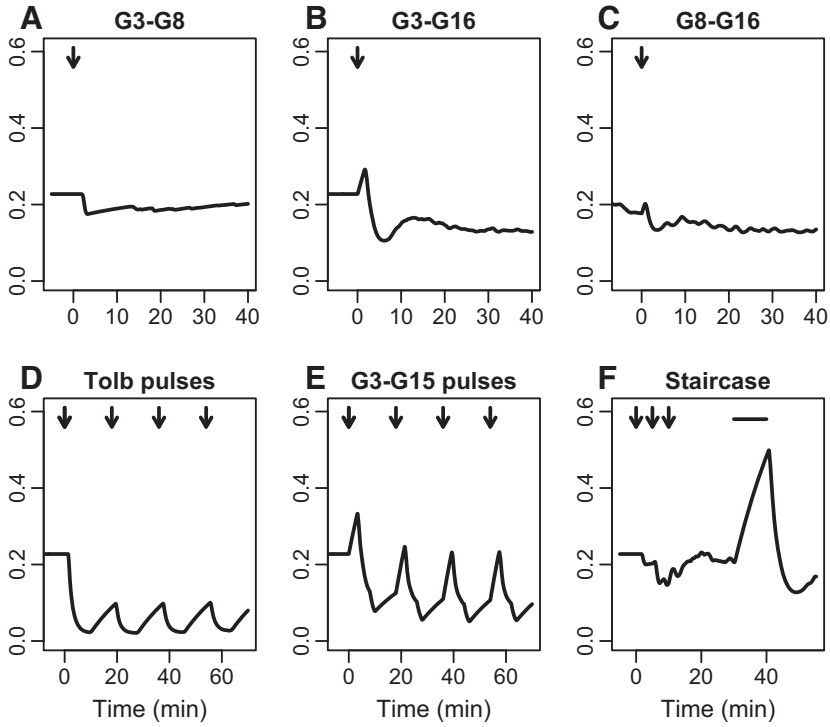

Fig. 4. Pool dynamics in Model 1. *A-F*: simulated dynamics of readily releasable pool (in % of islet content) obtained with Model 1 for 6 of the 14 protocols shown in Fig. 3. For protocol correspondence between the two figures refer to text, not to letter, above each panel. Tolb, tolbutamide.

sponse to tolbutamide and the relatively large first phase of secretion in response to glucose. We therefore analyzed the results with a slightly more complicated model.

Performance of Model 2

Compared with Model 1, Model 2 has an additional intermediate pool *X* between mobilization and the RRP (Fig. 1), which could correspond to docked but unprimed granules (9, 13, 16, 65). This model simulated most data sets well, except for the insulin peaks following glucose steps from 3 mM to 8.5 or 11.1 mM, which were much larger in the experiments compared with the simulated data (Fig. 5, *A* and *B*, red curves). This discrepancy was caused by the restrictions on the priming and mobilization rates, which were imposed to be nondecreasing functions of glucose. Indeed, when this constraint was removed, Model 2 was able to fit the data much better, which resulted in a U-shaped glucose dependence of the mobilization rate (Fig. 5, blue curves).

When priming and mobilization rates were constrained to be nondecreasing functions of the glucose concentration, the priming and refilling rates were estimated to be low (Fig. 5*O*). This assured that 8.5 mM glucose did not increase the RRP (Fig. 6*A*) to avoid that a subsequent rise in the $[Ca^{2+}]_i$ signal led to a too-large insulin peak when glucose was raised further (Fig. 5, *E–G*). Since the priming rate at 8.5 mM is small (Fig. 5*O*), precluding recruitment from the intermediate pool *X* (Fig. 6*A*, thin line), the simulated first phase at 8.5 mM glucose was small compared with the experiments (Fig. 5*A*).

The simulated first peak of insulin was larger upon stepping from 3 to 11.1 mM rather than 8.5 mM glucose (Fig. 5, *B* versus *A*) because the priming rate was increased. However, to fit the still low rate of second-phase secretion measured in 11.1 mM glucose, the increase in mobilization and priming rates had to be limited in the model (Fig. 5*O*). This explains why the simulated first peak remained lower than the experimental first phase (Fig. 5*B*). At higher glucose concentrations, the fits were excellent, except for a minor discrepancy when stepping from 8.5 mM to 30 mM glucose (Fig. 5*G*), in which the experimental trough following the first phase was absent in the model fit. This discrepancy is related to the rising second phase of secretion in the data, which the model is unable to capture. Similar to Model 1, the RRP and the pool *X* were nearly constant during 8.5 mM glucose stimulation (Fig. 6*A*). The smaller secretory responses to 16.7 or 30 mM glucose observed after pre-exposure to 8.5 rather than 3 mM glucose (Fig. 5, *F* and *G* versus *C* and *D*) were mainly due to differences in the Ca^{2+} responses.

Fits to experimental data obtained during constant or intermittent stimulations with tolbutamide or 15 mM glucose were excellent (Fig. 5, *H–K*). In particular, the second, third, and fourth pulses were reduced compared with the first ones (Fig. 5, *J* and *K*) because the intermediate pool *X* and the RRP only partially refilled between stimuli (Fig. 6, *D* and *E*). Also, the staircase experiments were reproduced very well (Fig. 5, *L* and *M*).

According to Model 2, estimated priming and mobilization rates were glucose-independent up to ~10 mM (Fig. 5*O*), suggesting that changes in the $[Ca^{2+}]_i$ profiles were entirely responsible for the differences in secretion within this physiologically relevant range.

Performance of Model 3

Model 3 has an additional glucose-independent path refilling the RRP. The model fit the data very well, even when priming and mobilization rates were constrained to increase with glucose (Fig. 7, red curves). No significant improvement was obtained when this assumption was relaxed (Fig. 7, blue curves). This model was able to reproduce the substantial

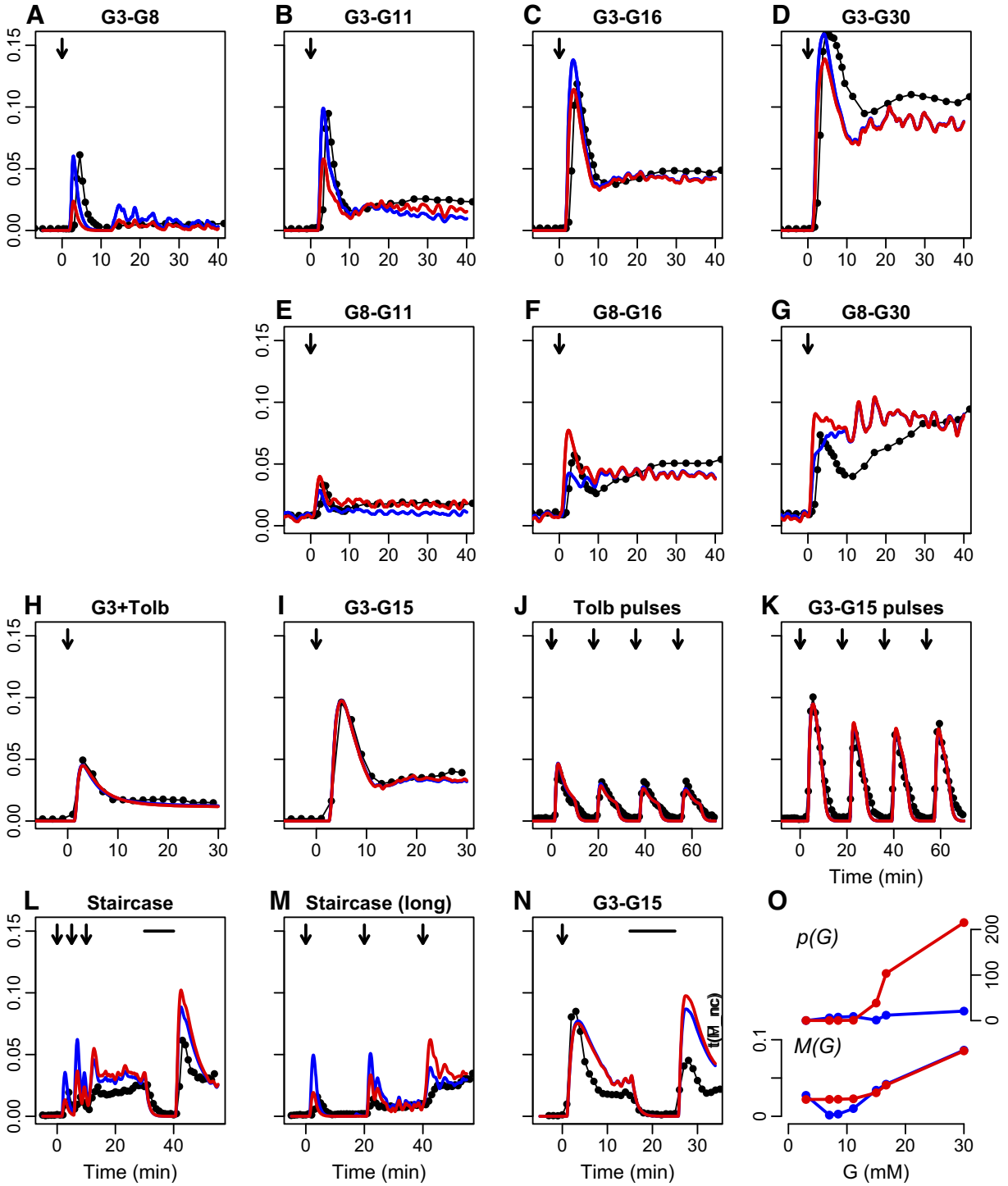

Fig. 5. Model 2 results. Simulated secretion profiles (% of islet content/min; axes are shown only once for each row) obtained with Model 2, fitted to the experimental data (black dots), either with (red curves) or without (blue curves) the constraint of refilling and priming being a nondecreasing function of the glucose concentration *G*. *A*–*N*: layout is the same as in Fig. 2. *O*: parameters for priming [$p(G)$ with unit 1/min; upper, right axis] and mobilization [$M(G)$ in % of islet content/min; lower, left axis] with (red) or without (blue) the monotony constraint on $p(G)$ and $M(G)$. $M(G)$, rate of glucose-dependent "refilling" process; p(G), glucose-dependent priming rate; Tolb, tolbutamide.

peaks of secretion when stepping from 3 mM to 8.5 or 11.1 mM glucose and above (Fig. 7, *A*–*D*). Stimulation with 8.5 mM glucose depleted the intermediate pool *X* almost completely (Fig. 8*A*), because priming was stimulated but refilling was not at this glucose level. Subsequent steps in glucose therefore led to smaller first-phase peaks, since first-phase secretion was mostly due to glucose-dependent recruitment of *X*. Thus, in contrast to the two previous models, Model 3 attributed to pool depletion (of *X*), a major role in explaining the differences following 3 mM or 8.5 mM pre-exposure.

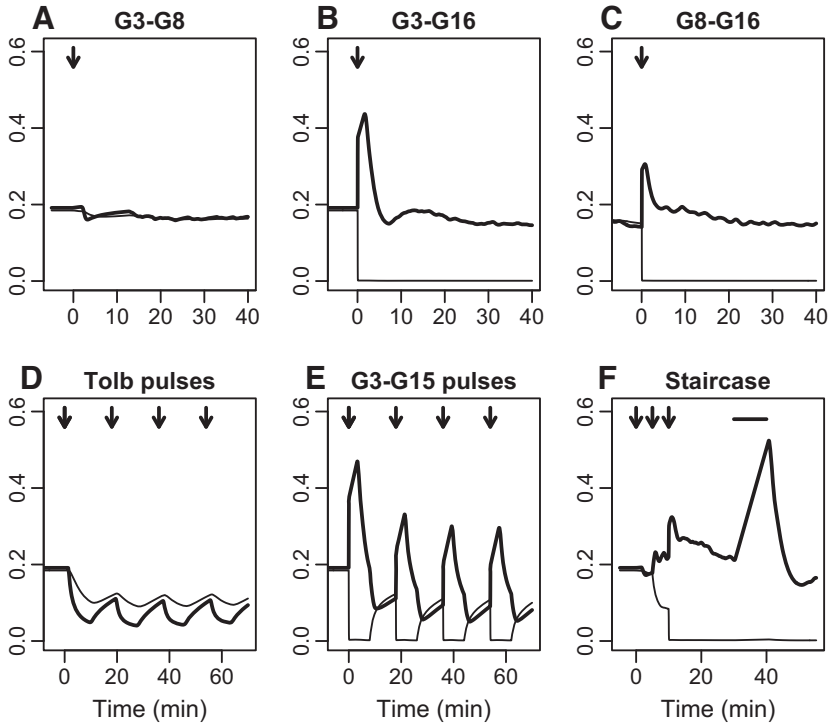

Fig. 6. Pool dynamics in Model 2. *A-F*: simulated dynamics of readily releasable pool (thick curves; % of islet content) and *X* (thin curves; % of islet content) obtained with Model 2 for 6 of the 14 protocols shown in Fig. 5. For protocol correspondence between the two figures refer to text, not to letter, above each panel. Tolb, tolbutamide.

As for Model 2, tolbutamide and staircase experiments were reproduced well, although Model 3 slightly overestimated the first peaks in response to the steps to 7 mM and 10 mM glucose (Fig. 7, *L* and *M*).

Compared with Model 2, the estimated priming rate increased with glucose already below 10 mM (Fig. 7*O*), suggesting that both granule and $[Ca^{2+}]_i$ dynamics played a role in shaping release patterns under physiological conditions. Indeed, depletion of *X* because of rapid priming (Fig. 8*A*) allowed the model to reproduce the peak of secretion already at 8.5 mM (Fig. 7*A*). These estimates for the glucose dependence of the priming rate in Model 3 correspond to experimental findings that amplification operates already at low glucose concentrations that do not increase $[Ca^{2+}]_i$ and, therefore, do not trigger insulin release on their own (25).

In contrast to Model 2, the pool size of *X* was nearly constant during tolbutamide simulations (Fig. 8*D*) since the additional direct refilling route allowed the model to refill the RRP between tolbutamide pulses with a very low priming rate *p* at 3 mM glucose. This, in turn, permitted a very low depriming rate *q*, which was estimated to be ~10-fold lower in Model 3 compared with Model 2. With lower *q* and basal *p*, Model 3 was able to create large simulated peaks when glucose was raised, by rapid glucose-dependent recruitment of the intermediate pool *X* (Fig. 8, *A*, *B*, and *E*). In other words, tolbutamide acted only on the RRP, whereas glucose acted on both *X* and RRP by recruiting *X* rapidly into the RRP, thereby causing the two pools to behave as if they were one. Amplification by higher concentrations of glucose was caused by increased mobilization of granules into *X*, followed by very rapid priming into the RRP.

DISCUSSION

Since it is notoriously more difficult to obtain long $[Ca^{2+}]_i$ recordings from human islets than mouse islets, and hence to study how calcium influences insulin secretion patterns through interactions with granule dynamics, we applied our modeling approach to previously published and novel data from mouse islets. Our analysis shows that both $[Ca^{2+}]_i$ changes and insulin granule pools contribute to biphasic secretion. Our findings give biological identity to the phenomenological signals proposed by Cerasi et al. (6) in the form of intracellular Ca^{2+}, whereas the pool description is virtually as suggested from experiments (2, 48).

The mathematical models presented here give a coherent framework for the integration of $[Ca^{2+}]_i$ and granule pools and are in some sense an updated version of an earlier signal-pool model (36). Notably, we did not assume any heterogeneity of the RRP, in contrast to some earlier pool models reproducing the staircase protocol (21, 50). Although our pool models are rather simple compared with previous detailed but less data-driven models of granule pool dynamics (4, 9, 51), they have the advantage of being driven by measured $[Ca^{2+}]_i$ profiles. Pedersen and Sherman (51) also included phasic and oscillatory "$[Ca^{2+}]_i$ profiles" consisting of square pulses but with no attention to the glucose dependency. Grespan et al. (20) similarly modeled calcium phenomenologically in combination with the description of a single granule pool.

Using Model 2 and Model 3, which fitted the data best, we can investigate the mechanisms creating the first phase of insulin release. Upon stimulation with moderately elevated glucose concentrations (<10 mM), the initial $[Ca^{2+}]_i$ peak is short and, in both models, a decline of the triggering signal terminates the first phase of secretion, although the RRP is still not completely depleted (Figs. 6*A* and 8*A*). A relevant difference between the two models is that, at moderate glucose levels, the intermediate pool *X* is left nearly untouched in Model 2 (Fig. 6*A*), whereas it is rapidly recruited into the RRP in Model 3 (Fig. 8*A*), which consequently allows this model to

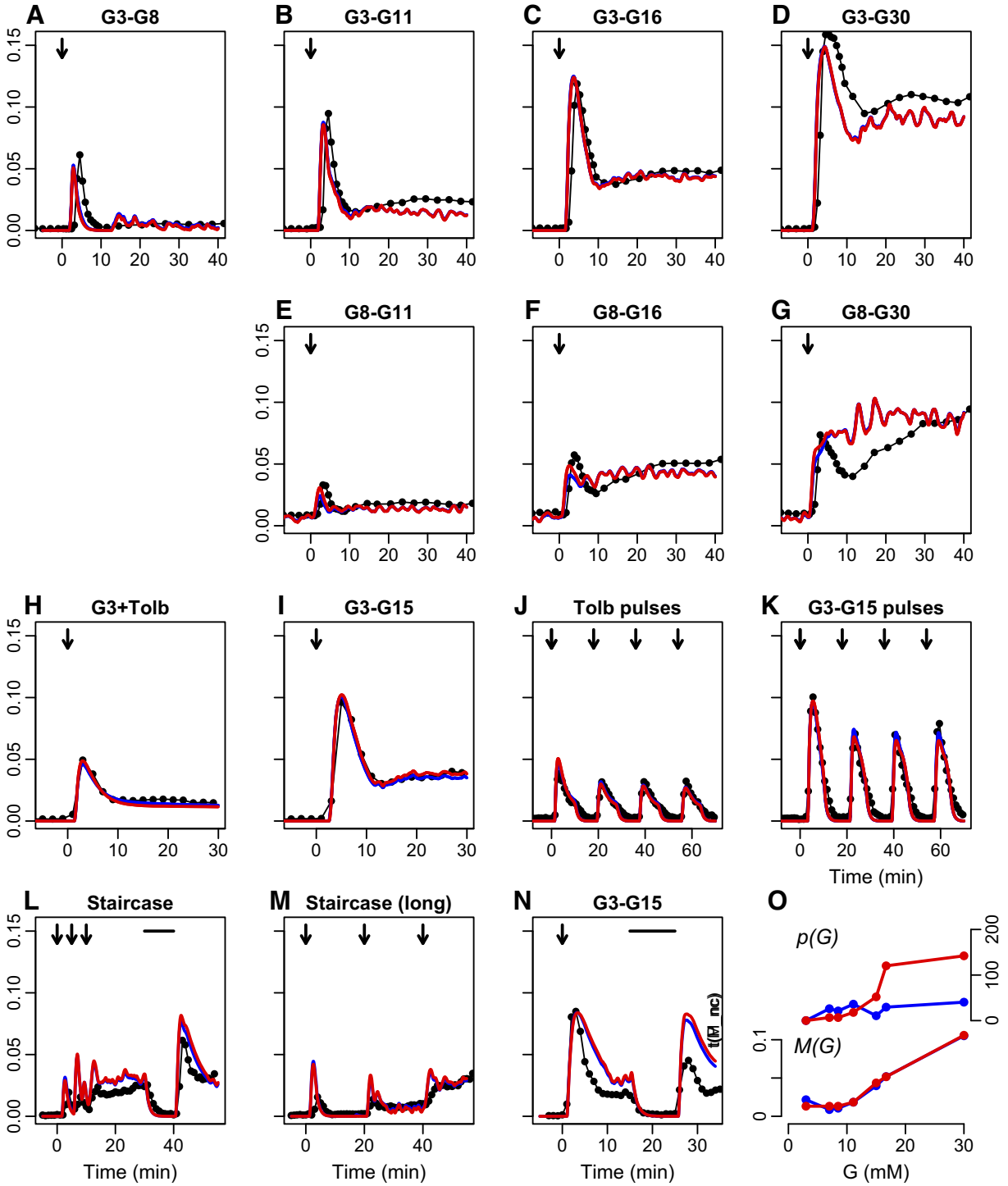

Fig. 7. Model 3 results. Simulated secretion profiles (% of islet content/min; axes are shown only once for each row) obtained with Model 3, fitted to the experimental data (black dots), either with (red curves) or without (blue curves) the constraint of refilling and priming being a nondecreasing function of the glucose concentration *G*. *A–N*: layout is the same as in Fig. 2. *O*: parameters for priming [$p(G)$ with unit 1/min; upper, right axis] and mobilization [$M(G)$ in % of islet content/min; lower, left axis] with (red) or without (blue) the monotony constraint on $p(G)$ and M(G). $M(G)$, rate of glucose-dependent "refilling" process; p(G), glucose-dependent priming rate; Tolb, tolbutamide.

create a larger insulin peak than Model 2 in response to moderate glucose concentrations.

At higher glucose concentrations, a longer first phase of $[Ca^{2+}]_i$ contributes to increase the first phase of secretion. However, secretion rates start to decline sooner than $[Ca^{2+}]_i$ (Fig. 2) (29), which might reflect progressive depletion of the RRP. In both models, the intermediate pool X is rapidly depleted by steps to glucose concentrations above 10 mM (Figs. 6*B* and 8*B*), which temporarily increases the size of the RRP and consequently augments the peaks of secretion. The

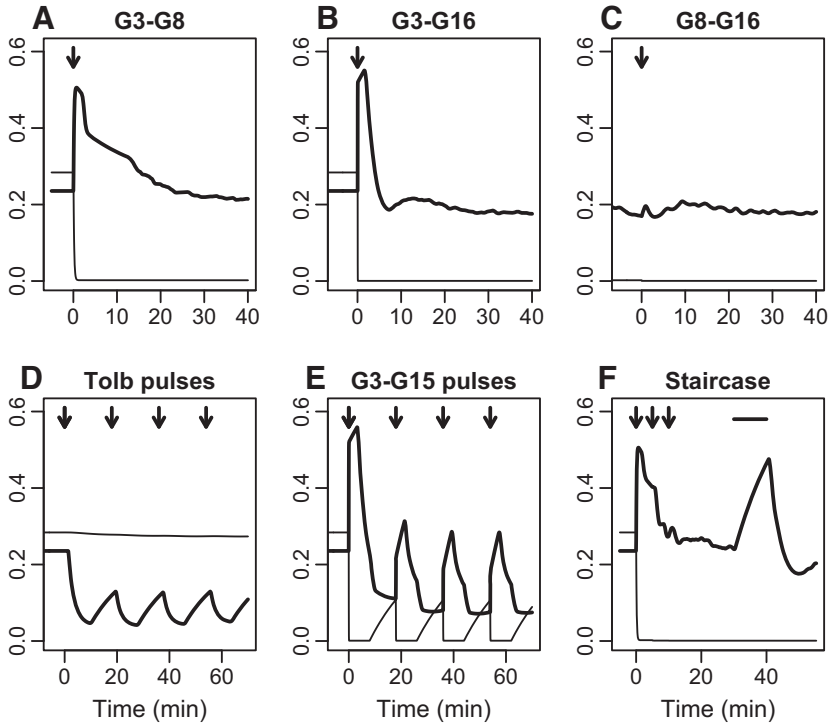

Fig. 8. Pool dynamics in Model 3. *A*-*F*: simulated dynamics of readily releasable pool (thick curves; % of islet content) and *X* (thin curves; % of islet content) obtained with Model 3 for 6 of the 14 protocols shown in Fig. 7. For protocol correspondence between the two figures refer to text, not to letter, above each panel. Tolb, tolbutamide.

secretion peak is then terminated by partial depletion of the RRP (Figs. 6*B* and 8*B*). In addition, granule "mobilization" toward pool *X* augments with glucose above 10 mM (Figs. 5*O* and 7*O*), which mainly permits setting of the second phase. Since $[Ca^{2+}]_i$ also increases with glucose, both mechanisms contribute to augment the second phase of secretion at higher glucose. Thus, both the $[Ca^{2+}]_i$ signal and refilling of the pool of releasable granules, which the signal acts on, are enhanced by glucose. In contrast, tolbutamide does not increase the size of the RRP but acts only via calcium.

The mechanisms generating phasic $[Ca^{2+}]_i$ changes in response to a glucose step are incompletely understood. Electrical activity is also biphasic under these conditions (24, 40, 42) and underlies the biphasic rise in $[Ca^{2+}]_i$. Based on the prominent role of $[Ca^{2+}]_i$ in driving the release patterns under the protocols investigated here, we encourage further studies on the mechanisms involved in shaping first-phase electrical and $[Ca^{2+}]_i$ responses in healthy and diabetic human β-cells.

Notably, we are able to simulate the staircase protocol without assuming any heterogeneity of the RRP. Each step of glucose is known to elicit a rapid increase in electrical activity (41) that causes a new $[Ca^{2+}]_i$ peak above the already elevated $[Ca^{2+}]_i$ (32). In response to the step to 7 mM glucose, the $[Ca^{2+}]_i$ peak is too short for complete depletion of granule pools (Figs. 4*F*, 6*F*, and 8*F*), and the trough following the first phase of secretion is due to fading of the triggering $[Ca^{2+}]_i$ signal, not to pool depletion. Hence, the RRP is still nearly filled when the next glucose step creates a new $[Ca^{2+}]_i$ peak, which therefore can produce another peak of insulin secretion. While this interpretation does not exclude that cell-to-cell heterogeneity (3), in particular with respect to $[Ca^{2+}]_i$ amplitude, amplifying signals, or the time-to-cell activation (32, 61), contributes to this pattern (21, 50), it highlights that the secretion profile of the staircase protocol can be largely explained by $[Ca^{2+}]_i$ dynamics. Further modeling studies should aim to investigate how cell-to-cell heterogeneity in combination with dynamic $[Ca^{2+}]_i$ patterns shape insulin secretion from a population of β-cells.

Glucose-dependent amplification of calcium-induced exocytosis is thought to account for 50% of insulin secretion during the 2 phases of insulin secretion in mouse (25, 43) and human islets (27). We suggest that amplification of first-phase insulin secretion is caused by glucose-dependent priming of granules located at or very close to the plasma membrane, likely by recruitment of exocytotic proteins to the insulin granules (1, 16, 18, 65). Second-phase amplification is attributed mostly to glucose-dependent "mobilization," in addition to rapid priming (17). It should, however, be kept in mind that amplification does not require a functional cytoskeleton and that "mobilization" does not imply long-distance transfer of granules (43, 44). The nature of the amplifying signals generated by glucose metabolism is still a matter of debate, but there is evidence for rapid ATP-dependent priming in single-cell recordings (14), and several other products have been suggested to be involved in the second-phase amplification (15, 33).

Detailed studies of the dynamics of insulin secretion by islets from subjects with type 2 diabetes have yet to be performed. However, perifusions of normal human islets have shown that increases in the prestimulatory glucose concentration from 3 mM to 6, 8 or 10 mM progressively decrease the magnitude of the first phase of insulin secretion induced by 15 mM glucose (26) but augment the response to tolbutamide (27). A decrease in first phase was also observed in mouse islets when stepping from 8 rather than 3 mM glucose to 16 mM (Fig. 2, *C* versus *F*). Our models indicate that both a smaller Ca^{2+} signal and, for Model 3, a reduced refilling of the RRP account for the phenomenon. We therefore only partly agree with a recent suggestion that defects in pool refilling

explain the loss of first-phase and the decrease of second-phase insulin secretion in subjects with type 2 diabetes, with no need to assume disturbed $[Ca^{2+}]_i$ handling (20). There is evidence that insulin granule docking and priming are disturbed in diabetic β-cells (17, 18). However, arginine (38, 53) and tolbutamide (34) remain able to induce a peak of insulin secretion in patients with diabetes and in isolated islets from diabetic donors (12), an effect mimicked by KCl-induced depolarization in single diabetic β-cells (10, 17). These results indicate that the RRP is not empty in diabetic β-cells. We therefore believe it is unlikely that the loss of biphasic insulin secretion in subjects with diabetes is the result of disturbed granule dynamics only. In contrast to tolbutamide, glucose is poorly able to induce electrical activity in diabetic compared with healthy β-cells (57), which most likely causes disturbed $[Ca^{2+}]_i$ dynamics and blunted insulin secretion (28, 57).

In summary, we propose that phasic $[Ca^{2+}]_i$ patterns contribute substantially to the creation of biphasic insulin secretion patterns, in addition to granule dynamics. Hence, to understand the cellular mechanisms that lead to disturbed biphasic insulin release in type 2 diabetes, better insight into the generation of phasic electrical activity and $[Ca^{2+}]_i$ dynamics in human β-cells is needed.

ACKNOWLEDGMENTS

The authors appreciate the contribution of Myriam Nenquin to the experimental aspects of the study.

GRANTS

M. G. Pedersen was supported by the University of Padova (Strategic Project "DYCENDI," and Project "SID 2017").

DISCLOSURES

No conflicts of interest, financial or otherwise, are declared by the authors.

AUTHOR CONTRIBUTIONS

M.G.P. conceived and designed research; M.G.P., A.T., and J.-C.H. performed experiments; M.G.P. and J.-C.H. analyzed data; M.G.P. and J.-C.H. interpreted results of experiments; M.G.P. prepared figures; M.G.P. drafted manuscript; M.G.P. and J.-C.H. edited and revised manuscript; M.G.P., A.T., and J.-C.H. approved final version of manuscript.

REFERENCES

1. **Alenkvist I, Gandasi NR, Barg S, Tengholm A.** Recruitment of Epac2A to insulin granule docking sites regulates priming for exocytosis. *Diabetes* 66: 2610–2622, 2017. doi:10.2337/db17-0050.
2. **Barg S, Eliasson L, Renström E, Rorsman P.** A subset of 50 secretory granules in close contact with L-type Ca^{2+} channels accounts for first-phase insulin secretion in mouse beta-cells. *Diabetes* 51, *Suppl* 1: S74–S82, 2002. doi:10.2337/diabetes.51.2007.S74.
3. **Benninger RKP, Hodson DJ.** New understanding of β-cell heterogeneity and in situ islet function. *Diabetes* 67: 537–547, 2018. doi:10.2337/dbi17-0040.
4. **Bertuzzi A, Salinari S, Mingrone G.** Insulin granule trafficking in β-cells: mathematical model of glucose-induced insulin secretion. *Am J Physiol Endocrinol Metab* 293: E396–E409, 2007. doi:10.1152/ajpendo.00647.2006.
5. **Blackard WG, Nelson NC.** Portal and peripheral vein immunoreactive insulin concentrations before and after glucose infusion. *Diabetes* 19: 302–306, 1970. doi:10.2337/diab.19.5.302.
6. **Cerasi E, Fick G, Rudemo M.** A mathematical model for the glucose induced insulin release in man. *Eur J Clin Invest* 4: 267–278, 1974. doi:10.1111/j.1365-2362.1974.tb02345.x.
7. **Cerasi E, Luft R.** The plasma insulin response to glucose infusion in healthy subjects and in diabetes mellitus. *Acta Endocrinol (Copenh)* 55: 278–304, 1967. doi:10.1530/acta.0.0550278.
8. **Cerasi E, Luft R, Efendic S.** Decreased sensitivity of the pancreatic beta cells to glucose in prediabetic and diabetic subjects. A glucose dose-response study. *Diabetes* 21: 224–234, 1972. doi:10.2337/diab.21.4.224.
9. **Chen YD, Wang S, Sherman A.** Identifying the targets of the amplifying pathway for insulin secretion in pancreatic beta-cells by kinetic modeling of granule exocytosis. *Biophys J* 95: 2226–2241, 2008. doi:10.1529/biophysj.107.124990.
10. **Cortese G, Gandasi NR, Barg S, Pedersen MG.** Statistical frailty modeling for quantitative analysis of exocytotic events recorded by live cell imaging: rapid release of insulin-containing granules is impaired in human diabetic β-cells. *PLoS One* 11: e0167282, 2016. doi:10.1371/journal.pone.0167282.
11. **Curry DL, Bennett LL, Grodsky GM.** Dynamics of insulin secretion by the perfused rat pancreas. *Endocrinology* 83: 572–584, 1968. doi:10.1210/endo-83-3-572.
12. **Del Guerra S, Lupi R, Marselli L, Masini M, Bugliani M, Sbrana S, Torri S, Pollera M, Boggi U, Mosca F, Del Prato S, Marchetti P.** Functional and molecular defects of pancreatic islets in human type 2 diabetes. *Diabetes* 54: 727–735, 2005. doi:10.2337/diabetes.54.3.727.
13. **Eliasson L, Abdulkader F, Braun M, Galvanovskis J, Hoppa MB, Rorsman P.** Novel aspects of the molecular mechanisms controlling insulin secretion. *J Physiol* 586: 3313–3324, 2008. doi:10.1113/jphysiol.2008.155317.
14. **Eliasson L, Renström E, Ding WG, Proks P, Rorsman P.** Rapid ATP-dependent priming of secretory granules precedes Ca^{2+}-induced exocytosis in mouse pancreatic B-cells. *J Physiol* 503: 399–412, 1997. doi:10.1111/j.1469-7793.1997.399bh.x.
15. **Ferdaoussi M, MacDonald PE.** Toward connecting metabolism to the exocytotic site. *Trends Cell Biol* 27: 163–171, 2017. doi:10.1016/j.tcb.2016.10.003.
16. **Gandasi NR, Barg S.** Contact-induced clustering of syntaxin and munc18 docks secretory granules at the exocytosis site. *Nat Commun* 5: 3914, 2014. doi:10.1038/ncomms4914.
17. **Gandasi NR, Yin P, Omar-Hmeadi M, Ottosson Laakso E, Vikman P, Barg S.** Glucose-dependent granule docking limits insulin secretion and is decreased in human Type 2 diabetes. *Cell Metab* 27: 470–478.e4, 2018. doi:10.1016/j.cmet.2017.12.017.
18. **Gandasi NR, Yin P, Riz M, Chibalina MV, Cortese G, Lund PE, Matveev V, Rorsman P, Sherman A, Pedersen MG, Barg S.** Ca^{2+} channel clustering with insulin-containing granules is disturbed in type 2 diabetes. *J Clin Invest* 127: 2353–2364, 2017. doi:10.1172/JCI88491.
19. **Gerich JE.** Is reduced first-phase insulin release the earliest detectable abnormality in individuals destined to develop type 2 diabetes? *Diabetes* 51, *Suppl* 1: S117–S121, 2002. doi:10.2337/diabetes.51.2007.S117.
20. **Grespan E, Giorgino T, Arslanian S, Natali A, Ferrannini E, Mari A.** Defective amplifying pathway of β-cell secretory response to glucose in Type 2 diabetes: integrated modeling of in vitro and in vivo evidence. *Diabetes* 67: 496–506, 2018. doi:10.2337/db17-1039.
21. **Grodsky GM.** A threshold distribution hypothesis for packet storage of insulin and its mathematical modeling. *J Clin Invest* 51: 2047–2059, 1972. doi:10.1172/JCI107011.
22. **Grodsky GM, Curry D, Landahl H, Bennett L.** [Further studies on the dynamic aspects of insulin release in vitro with evidence for a two-compartmental storage system]. *Acta Diabetol Lat* 6, *Suppl* 1: 554–578, 1969.
23. **Gromada J, Høy M, Renström E, Bokvist K, Eliasson L, Göpel S, Rorsman P.** CaM kinase II-dependent mobilization of secretory granules underlies acetylcholine-induced stimulation of exocytosis in mouse pancreatic B-cells. *J Physiol* 518: 745–759, 1999. doi:10.1111/j.1469-7793.1999.0745p.x.
24. **Henquin JC.** Regulation of insulin release by ionic and electrical events in B cells. *Horm Res* 27: 168–178, 1987. doi:10.1159/000180806.
25. **Henquin JC.** Regulation of insulin secretion: a matter of phase control and amplitude modulation. *Diabetologia* 52: 739–751, 2009. doi:10.1007/s00125-009-1314-y.
26. **Henquin JC, Dufrane D, Kerr-Conte J, Nenquin M.** Dynamics of glucose-induced insulin secretion in normal human islets. *Am J Physiol Endocrinol Metab* 309: E640–E650, 2015. doi:10.1152/ajpendo.00251.2015.
27. **Henquin JC, Dufrane D, Gmyr V, Kerr-Conte J, Nenquin M.** Pharmacological approach to understanding the control of insulin secretion in human islets. *Diabetes Obes Metab* 19: 1061–1070, 2017. doi:10.1111/dom.12887.

28. **Henquin JC, Ishiyama N, Nenquin M, Ravier MA, Jonas JC.** Signals and pools underlying biphasic insulin secretion. *Diabetes* 51, *Suppl* 1: S60–S67, 2002. doi:10.2337/diabetes.51.2007.S60.
29. **Henquin JC, Nenquin M, Stiernet P, Ahren B.** In vivo and in vitro glucose-induced biphasic insulin secretion in the mouse: pattern and role of cytoplasmic Ca^{2+} and amplification signals in β-cells. *Diabetes* 55: 441–451, 2006. doi:10.2337/diabetes.55.02.06.db05-1051.
30. **Hosker JP, Rudenski AS, Burnett MA, Matthews DR, Turner RC.** Similar reduction of first- and second-phase B-cell responses at three different glucose levels in type II diabetes and the effect of gliclazide therapy. *Metabolism* 38: 767–772, 1989. doi:10.1016/0026-0495(89)90064-4.
31. **Jonas JC, Gilon P, Henquin JC.** Temporal and quantitative correlations between insulin secretion and stably elevated or oscillatory cytoplasmic Ca^{2+} in mouse pancreatic β-cells. *Diabetes* 47: 1266–1273, 1998. doi:10.2337/diab.47.8.1266.
32. **Jonkers FC, Henquin JC.** Measurements of cytoplasmic Ca^{2+} in islet cell clusters show that glucose rapidly recruits β-cells and gradually increases the individual cell response. *Diabetes* 50: 540–550, 2001. doi:10.2337/diabetes.50.3.540.
33. **Kalwat MA, Cobb MH.** Mechanisms of the amplifying pathway of insulin secretion in the β cell. *Pharmacol Ther* 179: 17–30, 2017. doi:10.1016/j.pharmthera.2017.05.003.
34. **Karam JH, Sanz N, Salamon E, Nolte MS.** Selective unresponsiveness of pancreatic β-cells to acute sulfonylurea stimulation during sulfonylurea therapy in NIDDM. *Diabetes* 35: 1314–1320, 1986. doi:10.2337/diab.35.12.1314.
35. **Lacy PE, Walker MM, Fink CJ.** Perifusion of isolated rat islets in vitro. Participation of the microtubular system in the biphasic release of insulin. *Diabetes* 21: 987–998, 1972. doi:10.2337/diab.21.10.987.
36. **Landahl HD, Grodsky GM.** Comparison of models of insulin release. *Bull Math Biol* 44: 399–409, 1982. doi:10.1007/BF02462288.
37. **Lenzen S.** Insulin secretion by isolated perfused rat and mouse pancreas. *Am J Physiol* 236: E391–E400, 1979. doi:10.1152/ajpendo.1979.236.4.E391.
38. **Lim EL, Hollingsworth KG, Aribisala BS, Chen MJ, Mathers JC, Taylor R.** Reversal of type 2 diabetes: normalisation of beta cell function in association with decreased pancreas and liver triacylglycerol. *Diabetologia* 54: 2506–2514, 2011. doi:10.1007/s00125-011-2204-7.
39. **Low JT, Mitchell JM, Do OH, Bax J, Rawlings A, Zavortink M, Morgan G, Parton RG, Gaisano HY, Thorn P.** Glucose principally regulates insulin secretion in mouse islets by controlling the numbers of granule fusion events per cell. *Diabetologia* 56: 2629–2637, 2013. doi:10.1007/s00125-013-3019-5.
40. **Mears D, Sheppard NF Jr, Atwater I, Rojas E, Bertram R, Sherman A.** Evidence that calcium release-activated current mediates the biphasic electrical activity of mouse pancreatic β-cells. *J Membr Biol* 155: 47–59, 1997. doi:10.1007/s002329900157.
41. **Meissner HP.** Electrical characteristics of the beta-cells in pancreatic islets. *J Physiol (Paris)* 72: 757–767, 1976.
42. **Meissner HP, Atwater IJ.** The kinetics of electrical activity of β cells in response to a "square wave" stimulation with glucose or glibenclamide. *Horm Metab Res* 8: 11–16, 1976. doi:10.1055/s-0028-1093685.
43. **Mourad NI, Nenquin M, Henquin JC.** Metabolic amplifying pathway increases both phases of insulin secretion independently of β-cell actin microfilaments. *Am J Physiol Cell Physiol* 299: C389–C398, 2010. doi:10.1152/ajpcell.00138.2010.
44. **Mourad NI, Nenquin M, Henquin JC.** Metabolic amplification of insulin secretion by glucose is independent of β-cell microtubules. *Am J Physiol Cell Physiol* 300: C697–C706, 2011. doi:10.1152/ajpcell.00329.2010.
45. **Nijpels G, Boorsma W, Dekker JM, Hoeksema F, Kostense PJ, Bouter LM, Heine RJ.** Absence of an acute insulin response predicts onset of type 2 diabetes in a Caucasian population with impaired glucose tolerance. *J Clin Endocrinol Metab* 93: 2633–2638, 2008. doi:10.1210/jc.2007-2837.
46. **Nunemaker CS, Wasserman DH, McGuinness OP, Sweet IR, Teague JC, Satin LS.** Insulin secretion in the conscious mouse is biphasic and pulsatile. *Am J Physiol Endocrinol Metab* 290: E523–E529, 2006. doi:10.1152/ajpendo.00392.2005.
47. **O'Connor MD, Landahl H, Grodsky GM.** Comparison of storage- and signal-limited models of pancreatic insulin secretion. *Am J Physiol* 238: R378–R389, 1980. doi:10.1152/ajpregu.1980.238.5.R378.
48. **Olofsson CS, Göpel SO, Barg S, Galvanovskis J, Ma X, Salehi A, Rorsman P, Eliasson L.** Fast insulin secretion reflects exocytosis of docked granules in mouse pancreatic B-cells. *Pflugers Arch* 444: 43–51, 2002. doi:10.1007/s00424-002-0781-5.
49. **Pedersen MG, Bertram R, Sherman A.** Intra- and inter-islet synchronization of metabolically driven insulin secretion. *Biophys J* 89: 107–119, 2005. doi:10.1529/biophysj.104.055681.
50. **Pedersen MG, Corradin A, Toffolo GM, Cobelli C.** A subcellular model of glucose-stimulated pancreatic insulin secretion. *Philos Trans Royal Soc A Math Phys Eng Sci* 366: 3525–3543, 2008. doi:10.1098/rsta.2008.0120.
51. **Pedersen MG, Sherman A.** Newcomer insulin secretory granules as a highly calcium-sensitive pool. *Proc Natl Acad Sci USA* 106: 7432–7436, 2009. doi:10.1073/pnas.0901202106.
52. **Pfeifer MA, Halter JB, Porte D Jr.** Insulin secretion in diabetes mellitus. *Am J Med* 70: 579–588, 1981. doi:10.1016/0002-9343(81)90579-9.
53. **Porte D Jr.** Banting lecture 1990. Beta-cells in type II diabetes mellitus. *Diabetes* 40: 166–180, 1991. doi:10.2337/diab.40.2.166.
54. **Pratley RE, Weyer C.** The role of impaired early insulin secretion in the pathogenesis of Type II diabetes mellitus. *Diabetologia* 44: 929–945, 2001. doi:10.1007/s001250100580.
55. **Ravier MA, Güldenagel M, Charollais A, Gjinovci A, Caille D, Söhl G, Wollheim CB, Willecke K, Henquin JC, Meda P.** Loss of connexin36 channels alters beta-cell coupling, islet synchronization of glucose-induced Ca^{2+} and insulin oscillations, and basal insulin release. *Diabetes* 54: 1798–1807, 2005. doi:10.2337/diabetes.54.6.1798.
56. **Ricordi C, Lacy PE, Finke EH, Olack BJ, Scharp DW.** Automated method for isolation of human pancreatic islets. *Diabetes* 37: 413–420, 1988. doi:10.2337/diab.37.4.413.
57. **Rorsman P, Ashcroft FM.** Pancreatic β-cell electrical activity and insulin secretion: of mice and men. *Physiol Rev* 98: 117–214, 2018. doi:10.1152/physrev.00008.2017.
58. **Rorsman P, Braun M.** Regulation of insulin secretion in human pancreatic islets. *Annu Rev Physiol* 75: 155–179, 2013. doi:10.1146/annurev-physiol-030212-183754.
59. **Smolen P, Rinzel J, Sherman A.** Why pancreatic islets burst but single β cells do not. The heterogeneity hypothesis. *Biophys J* 64: 1668–1680, 1993. doi:10.1016/S0006-3495(93)81539-X.
60. **Speier S, Gjinovci A, Charollais A, Meda P, Rupnik M.** Cx36-mediated coupling reduces β-cell heterogeneity, confines the stimulating glucose concentration range, and affects insulin release kinetics. *Diabetes* 56: 1078–1086, 2007. doi:10.2337/db06-0232.
61. **Stožer A, Dolenšek J, Rupnik MS.** Glucose-stimulated calcium dynamics in islets of Langerhans in acute mouse pancreas tissue slices. *PLoS One* 8: e54638, 2013. doi:10.1371/journal.pone.0054638.
62. **Stumvoll M, Fritsche A, Häring HU.** Clinical characterization of insulin secretion as the basis for genetic analyses. *Diabetes* 51, *Suppl* 1: S122–S129, 2002. doi:10.2337/diabetes.51.2007.S122.
63. **Toschi E, Camastra S, Sironi AM, Masoni A, Gastaldelli A, Mari A, Ferrannini E, Natali A.** Effect of acute hyperglycemia on insulin secretion in humans. *Diabetes* 51, *Suppl* 1: S130–S133, 2002. doi:10.2337/diabetes.51.2007.S130.
64. **Weiss R, Caprio S, Trombetta M, Taksali SE, Tamborlane WV, Bonadonna R.** β-cell function across the spectrum of glucose tolerance in obese youth. *Diabetes* 54: 1735–1743, 2005. doi:10.2337/diabetes.54.6.1735.
65. **Yasuda T, Shibasaki T, Minami K, Takahashi H, Mizoguchi A, Uriu Y, Numata T, Mori Y, Miyazaki J, Miki T, Seino S.** Rim2alpha determines docking and priming states in insulin granule exocytosis. *Cell Metab* 12: 117–129, 2010. doi:10.1016/j.cmet.2010.05.017.